15

Highly sensitive express nonlinear optical diagnostics of the crystalline state of heterostructures such as sphalerite

© M.F. Stupak,[1,3] N.N. Mikhailov,[2,3] S.A. Dvoretsky,[2,4] S.N. Makarov,[1] A.G. Yelesin,[1] A.G. Verhoglyad[1]

[1] Technological Design Institute of Scientific Instrument Engineering, Siberian Branch of the Russian Academy of Sciences (TDI SIE SB RAS),
630058, Novosibirsk, Russia
[2] The Institute of Semiconductor Physics, Siberian Branch of the Russian Academy of Sciences (ISP SB RAS),
630090, Novosibirsk, Russia
[3] Novosibirsk State University (NSU),
630090, Novosibirsk, Russia
[4] Tomsk State University (TSU),
634050, Tomsk, Russia
e-mail: stupak@tdisie.nsc.ru

Received February 13, 2021
Revised May 16, 2021
Accepted June 11, 2021

The characteristics of a highly sensitive express bench for nonlinear optical diagnosis of crystalline structures such as sphalerite by generation of the second harmonica are presented. The analysis of the possibilities of quantitative and qualitative characterization of the features of the crystalline parameters of the layers of heteroepitaxial structures $Cd_xHg_{1-x}Te$ on substrates from GaAs with orientation (013) was carried out. The results were obtained by deviations of orientation in layers from the orientation of the substrate, which arose during the epitaxy, to determine the existence of stresses. The high sensitivity of the bench revealed the presence/absence of micro-particles with a disordered crystalline structure. Experimental results of reversible modification of the „in situ" crystalline state of $Cd_xHg_{1-x}Te$ structures with short-term local radiation exposure of high power laser radiation are given. New experimental data have been presented showing that the components of the nonlineaic susceptibility tensor $\chi_{xyz}(\omega)$ of the crystalline structure of $Cd_xHg_{1-x}Te$ depend on composition and are an order of magnitude larger than similar components of tensor in CdTe and GaAs.

Keywords: sphalerite crystals, second harmonica, azimuth angular dependence, tensor of nonlinear susceptibility, tensions, microparticle, radiation heating, heterostructures $Cd_xHg_{1-x}Te$.

DOI: 10.21883/TP.2022.14.55233.34-21

Introduction

In order to determine the structural perfection of the crystals and their defects, well-established methods are applied, based on the diffraction of X-rays, electron and neutron beams. Those are high-sensitivity methods. However, their implementation requires special equipment, personnel protection, besides, special techniques should be applied for sample preparation for the research. A separate issue for those methods is the creation of small zones for substance control. For example, the depth of X-rays penetration can make hundreds of microns.

Over three decades ago, an effective method was proposed and explored of diagnosing crystalline perfections of noncentrosymmetric crystals — a second harmonic generation method (SHG) [1]. The SH generation as a method of crystal structure control turns out to be a faster and more convenient investigation method for obtaining express information as compared to the traditional electronic, X-ray and other diffraction methods. The dependence of SHG components polarization intensity on the mutual orientation of the exciting radiation polarization relative to the crystallophysical axes, when the SH polarization, parallel or perpendicular to the azimuthally varying linear polarization of the exciting radiation (further as the text goes — angular or azimuthal dependence) is registered, allows obtaining quantitative information about the crystalline state of the surface layer, its orientation and several other properties while comparing experimental and model data in a given local area, to an accuracy less than or equal to a degree [1–11]. The diagnostic capabilities of the SHG method are widely used, for example, when studying the electronic and magnetic properties of materials by the characteristics the of identified magnetically induced second optic harmonic generation in diamagnetic and paramagnetic semiconductors [12,13].

Note that the SHG method allows obtaining data from a large area with high local resolution in the near-surface layer of the crystal [5,14], when moving a focused laser beam along two coordinates of the sample surface.

Increasing the SHG method sensitivity allows revealing specific properties of the fine structure of crystalline perfection, especially for multicomponent and multilayer structures. Such type of structures comprises MBE-grown heteroepitaxial layers (HEL) of cadmium and mercury

telluride (MCT, HgCdTe), on GaAs and Si substrates, of sphalerite symmetry or zinc blend class. Obtaining those structures of high quality for subsequent practical applications in IR detectors [15] requires resolving the issues associated with a large lattice mismatch and non-isovalency of conjugated materials of MCT alloys and GaAs and Si [16] substrates. Various research techniques detected multiple lattice damages and their link to the growth conditions [17–21]. Earlier studies using the second harmonic generation of probing radiation allowed determining the orientation and crystalline state of the layers in MCT MBE heteroepitaxial structure on (013)GaAs substrates, and demonstrated high efficiency of the SH method in experimental testing of high-quality heterostructures creation mode [9–11]. The data obtained allow predicting the application of the SHG method for investigating the quality of the consecutive stages of MBE-technology-based growing of MCT heteroepitaxial structure layers to determine the optimal conditions of the processes and requirements to the substrate. However, enhancing the approach to investigation of crystalline structure, damages to that and observation of finer effects requires higher sensitivity of nonlinear optical diagnostics.

The purpose of this work is to present the characteristics of a high-sensitivity express bench for nonlinear optical diagnostics (NLOD) and to present the results of its application for more meaningful characterization of the crystalline quality of MCT MBE heteroepitaxial structure and the substrate material of those structures in SH generation for reflection, to obtain new information about the presence/absence of structures and substrate stress, to detect disoriented microareas, reversible radiation and to evaluate tensor relations $\chi_{xyz}(\omega)$ in the MCT layers and GaAs substrate.

1. Charateristics of excitation and registration of SHG signals in GaAs, CdTe, MCT crystals

The calculation of the SHG signal intensity determined by the components of the nonlinear susceptibility tensor $\chi_{xyz}(\omega)$ in sphalerite class crystals (class $\bar{4}3m$ in international classification) is described in detail in [1,2]. For comparing the predicted data and experimental results of the SHG signal azimuthal dependences behavior in a specific geometry and for specific crystal slices, computer modelling [3,5,11] is applied.

For MBE-technology-based growing of MCT heterostructures, we use GaAs substrates with (013) orientation. To maintain the orientation and to resolve the issue of a large 13.6% mismatch between the GaAs lattice and MCT parameters, buffer layers of ZnTe and CdTe are grown sequentially. Thus, an „alternative" CdTe/ZnTe/GaAs substrate is prepared that maintains the orientation (013) and ensures a significantly smaller mismatch of lattice parameters with MCT (below 0.3%).

For the components of MCT heterostructures, such as GaAs substrate, CdTe and ZnTe layers, exiting radiation absorption $\sim 1\mu$m can be neglected, with due account for Fresnel reflectance losses only. The analysis of reference and literature reports on the optical characteristics of semiconductor materials demonstrates significantly scattered values of reflection factors, permittivity, absorbability, this being explained by different technologies for obtaining the test material, different conditions of setting up and conducting experiments, and different practices of sample surface treatment.

Especially important is the sample surface condition in the area of fundamental absorption while the light interacts with the matter in a very thin near-surface layer [22]. In the fundamental absorption area at the second harmonic wavelength ($\lambda = 0.53\,\mu$m) the penetration depth according to the reference and our data makes ~ 130 nm for CdTe, ~ 140 nm for GaAs and ~ 210 nm for ZnTe [14]. Those figures are in a satisfactory fit with reference and literature data [22–24]. The MCT layers are opaque both for the exciting radiation at $\lambda = 1.064\,\mu$m, and for its second harmonic. For the visible range, the depth of penetration depends significantly on the composition of the MCT upper layer [23,24]. The penetration depth, as measured by us, for the upper graded band-gap base of our heterostructures within the range in the area of $1\,\mu$m does not exceed $0.2\,\mu$m, the SHG absorption length making $\leq 0.03\,\mu$m, which agrees well with the data [23,24]. This means that in our experiments, the SHG signals from the MCT heterostructure and from the GaAs substrate of this heterostructure are purely reflected.

Given the interference nature of the reflected second harmonic, its effective generation depth is determined in a transparent medium by its coherent length of $d \approx \lambda/4\pi n(\omega)$, with strong absorption the generation depth d is determined by the minimum values of $\alpha^{-1}(\omega)$ and $\alpha^{-1}(2\omega)$ [1], where λ is the wavelength of the basic radiation, n is the refraction index of the medium at that wavelength, α is the respective absorption factors at the basic and doubled frequencies. In intermediate cases of weak absorption, the exact formula: $d = \lambda/4(n(\omega) + n(2\omega))$ [25,26] should be used to determine the effective depth of generation. The evaluations showed that the diagnostic depth of the tested HgCdTe samples in the report is determined by the value of $\alpha^{-1}(2\omega)$, the depth of SHG generation reflected from GaAs substrates and CdTe layers is determined by the coherent length making $\sim 25-20$ nm. MCT and GaAs substrates is determined only by the value of $\alpha^{-1}(2\omega)$.

Our analysis in [14] of the behavior of the SHG signal model azimuthal dependences plots (SHG polarization is parallel or perpendicular to the azimuthally varying linear polarization of the exciting radiation) with variation in terms of Θ and φ angles near (013) orientation demonstrated that those dependences are most sensitive to minor deviations from φ angle at normal beam incidence. Therefore, in order to achieve high sensitivity of the SHG method when determining the orientation of the tested near-surface

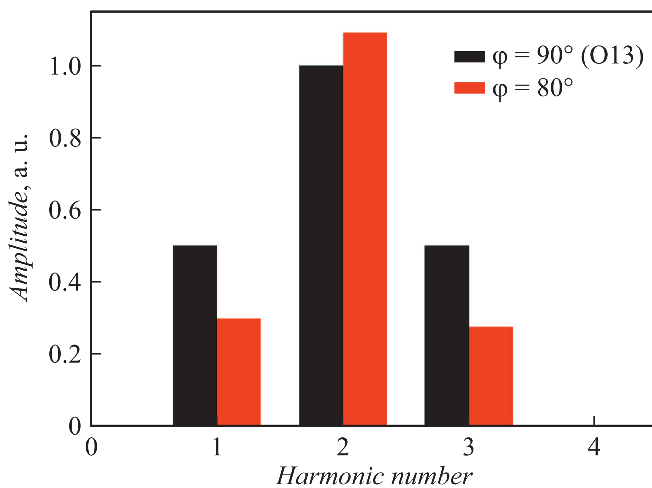

Figure 1. Fourier analysis of the model azimuthal dependences of the SHG intensity for the normal incidence with the shear variation near (013) for the angle of φ.

layer at the non-linear optical test bench, w frequency laser radiation is incident normally on the sample, with simultaneous plane-of-polarization rotation (azimuth angle) of exciting radiation in the range from 0 to 359° and registration of the signal intensity of reflected SHG with polarization, parallel or perpendicular to laser radiation polarization. Although all the necessary information on the SHG signal azimuthal dependence diagrams is located within the range of 0–179°, and further, mere repetition of the graph follows, experimentalists use the range from 0 to 359° with the express aim of controlling that repeatability because of possible aperture errors of the experimental facility when aligning both the optical path of the SHG signal passing to the receiving equipment, and the path of the exciting laser radiation passing through the rotating plate $\lambda/2$.

Fourier analysis of the model azimuthal dependences near the shear (013) of the sphalerite-type heterostructure is shown in Fig. 1 and demonstrates the presence of only the first, second and third harmonics with their amplitudes and phases (see [1]). In the simulation, the Θ and φ angles reference is the base shear (100). The Fourier-harmonics amplitude is presented in relative units, the polarization of the reflected SHG is parallel to the polarization of the laser exciting radiation.

It should be emphasized that the SHG signal azimuthal dependence diagram for a perfectly accurate orientation (013) at an angle of $\varphi = 90°$ should demonstrate the same amplitudes of all the four maxima. It was demonstrated that the SHG signal variations for the Θ angle (at a fixed angle of $\varphi = 90°$) near shear (013) result in almost identical changes of the amplitude of the diagrams of SHG intensity dependence on the azimuthal angle with the relations between the maxima [14] unchanged.

When diagnosing semiconductor materials and structures that are transparent to the main radiation, the value of the registered reflected SHG signal at a given level of laser exciting radiation depends on the characteristics of the crystal, the perfection of its near-surface layer and on volume stresses (induced birefringence), the reflection of exciting radiation from the sample rear surface at the control point [3,5,11]. When studying the GaAs substrates and the CdTe buffer layers, given the strong absorption at the second harmonic frequency in those semiconductor materials transparent for the main radiation, it can be stated that the SHG signal corresponds to the point symmetry group of the near-surface layer crystal and can be thus used to characterize the structural quality of the 0.3–1 μm thick layer. The SHG signal value in this case may exceed, by an order of magnitude, the value of the SHG signal [5,11] reflected from the front surface alone. Since the MCT layers are opaque to the exciting radiation ($\lambda = 1.064\,\mu$m) and to its second harmonic, there exists a unique possibility of recording only the reflected SH, both from the MCT surface layer in the heterostructure and from the substrate backside. GaAs substrates had a double-sided polishing. This allows making a comparative analysis of the nonlinear susceptibilities of those materials, diagnosing a comparative presence of stresses in the substrate and in the MCT heterostructure layers.

Thus, the quality assessment criterion of the crystal state in a given local region of the tested sample surface upon the analysis of the measured azimuthal dependences is:

(a) identifying correspondence to a certain point symmetry group and determining the absolute orientation of the local crystal region, with the required accuracy, relative to the sample surface;

b) identifying the presence of stresses in that region; c) qualitative assessment of the level of defects by a comparative analysis of SHG signal amplitudes (along the surface or for the same type of samples).

2. High-Sensitivity laboratory bench for nonlinear optical diagnostics

A detailed description of the heterostructure and operation of the nonlinear optical diagnostics (NLOD) laboratory bench consisting of a laser source, an optical-mechanical unit, power supply units and a control computer-based data reception and processing unit is given in [14]. As an emitter, a DUETTO-OEM V3.4 pulsed-periodic diode-pumped YAG:Nd-laser is used, with the wavelength of 1.064 μm, 50 kHz repetition rate of the pulse train of $sim10$ pulses, with a pulse duration of $sim10$ ps. The laser radiation is focused by a long-focus lens to the surface of the test sample into a spot of 200 μm in diameter according to the required spatial resolution. The $\lambda/2$ plate rotates according to a preset program around the laser beam axis by a stepper motor and rotates the plane of polarization of the radiation incident normally on the sample. A specialized parametric mirror (transmitting laser radiation and reflecting its second harmonic at the angle of incidence of 45°)

separates the SHG signal in the radiation reflected from the sample and further, through an analyzer, which orientation is synchronized with the orientation of $\lambda/2$ plate, and a light filter that only transmits SHG radiation, sends the SHG signal through the optical waveguide to the PMT-130.

We upgraded the bench that underwent targeted changes thus allowing to reduce the existing noises by over an order of magnitude and to increase the level of the valid SHG signal and thereby enhance the sensitivity. That was achieved mainly through the frequency selection and enhancement of the valid signal after the photomultiplier tube.

The PMT signal was then fed to a UNIPAN-233 selective amplifier-nanovoltmeter tuned to the operating frequency of the repetitively-pulsed YAG:Nd-laser equal to 50 kHz. Afterwards, the frequency-selected and enhanced signal was fed to the ADC module and continuously read out by the specialized software installed in a personal computer.

Enhanced bench sensitivity allowed to reduce the average power of probing laser radiation. In the experimental findings presented below, the average power varied from 10 to 70 mW. The standard time for obtaining an experimental diagram of the angular dependence of the SHG signal ranged from 10 to 30 s. Enhanced sensitivity of the NOLD bench by almost two orders of magnitude led to recording a percent proportion of the SHG signal passed through a parametric mirror, produced in the $\lambda/2$ quartz plate, so a cut-off light filter KC-17 was placed in the receiving path of the bench after the quartz plate $\lambda/2$.

The receiving equipment of the bench recorded the signal of the reflected SHG intensity with polarization parallel to the polarization of the laser radiation polarization, all the experimental results in the report correspond to that configuration.

Structurally, the optical-mechanical unit of the NOLD bench is put on the optical plate of the laser source in a small ($50 \times 50 \times 25$ cm) light-tight casing with inlet and outlet openings for the working radiation; an easily replaceable casing of the sample attachment and adjustment unit is docked to the outlet opening. This allowed organizing the normal operation of the NOLD complex in a laboratory setting in normal ambient lighting conditions, and the replacement and adjusting of the test sample took less than five minutes.

The standard deviation of the noise signal (with zero mean) corresponded to about 16 ADC code units, the level of the characteristic amplitude of the SH signal on the diagrams was within the range of 2000–4500 ADC code units.

The comparison error of the experimental and model angular dependences of the SHG signal on the samples made one degree for φ angle. The principal quantitative parameter of the NOLD method used is the determination, to a required accuracy, of the absolute orientation of the local crystalline region with respect to the sample surface. In our case, the accuracy is determined by the „frequency" of the comparison grid in terms of the Θ and φ angles of the model azimuthal dependences with the experimental diagram. The programmed grid step is chosen to be 1° for the φ angle. If necessary, in case of weak stresses, the comparison grid step for the Θ and φ angles of the model azimuthal dependences can be chosen equal to 0.1°, then the absolute orientation accuracy increases by an order of magnitude. Comparative analysis of the amplitudes of the experimental SHG signal (along the surface or for the same type of samples) can be carried out with an error below 0.05. Thus, the changed number of nonlinear dipoles associated with the changes in the density of various defects can be fixed with an error of 0.05. The presence/absence of stresses is detected, with the same error, for raising some minima of the experimental diagram of the azimuthal dependence.

3. Crystalline state characterization of MCT layers and structures, GaAs substrates with the help of the NOLD bench

3.1. Assessment of tensor $\chi_{xyz}(\omega)$ ratios in MCT and GaAs structures. Consideration of the re-reflected waves factor

The layers and substrate of MBE-grown $Cd_xHg_{1-x}Te$(MCT)/CdTe/ZnTe/GaAs heterostructures using „Ob-M" unit were studied. ZnTe and CdTe buffer layers of 30 nm and 5.5 μm in thickness were grown sequentially on (013)GaAs semi-insulating substrates. $Cd_xHg_{1-x}Te$ layers consisted of a $\sim 6\,\mu$m thick absorbing layer of $x = 0.22$ composition, with wide band graded gap layers bases at absorber layer boundaries, in which the composition changed smoothly from $x = 0.45$ to 0.22 at the initial stage of MCT growth at $\sim 1.5\,\mu$m thickness (inner graded band-gap base) and at its termination, from $x = 0.22$ to 0.45 at $\sim 0.5\,\mu$m thickness (upper graded band-gap base).

We recorded a significantly higher SHG signal amplitude from the outer $Cd_{0.45}Hg_{0.55}Te$ graded gap layer on the surface of the $Cd_xHg_{1-x}Te$/CdTe/ZnTe/GaAs heterostructure as compared to the underlying CdTe buffer layers and GaAs substrate [14]. The results testify that in this case the components of the $\chi_{xyz}(\omega)$ nonlinear susceptibility tensor of the crystal heterostructure are significantly larger than similar tensor components in CdTe and GaAs. In the measurements on the high-sensitivity NOLD bench as part of the subsequent experiments at the fixed level of recording equipment sensitivity (power supply to PMT, selective nanovoltmeter, ADC preamplifier) and the same level of IR exciting radiation (average power of radiation at $\lambda = 1.064\,\mu$m was 0.06 W) the amplitude of the signal reflected from the upper graded band-gap base of the second harmonic MCT was also significantly greater as compared to the similar SHG signals from the CdTe, ZnTe layers or from the back side of the GaAs substrate. We took

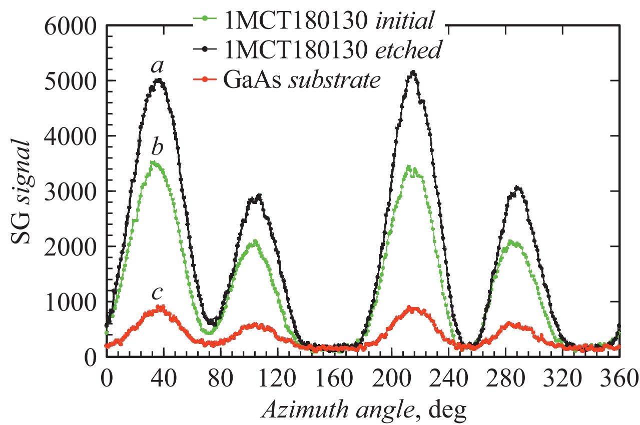

Figure 2. Experimental diagrams of the azimuthal dependence of the SHG signal amplitude on the MCT180130 heterostructure: a — from the outer graded band-gap base; b — after removal of the outer graded band-gap base; c — from the back side of the GaAs substrate. The average power of radiation at $\lambda = 1.064\,\mu$m made 0.06 W. The orientation of a and b layers is different from (013) in terms of φ angle by -5°, the orientation of the substrate is different from (013) in terms of φ angle by -3°. The polarizations of SHG and laser radiation are parallel.

the same measurements upon removing the outer graded band-gap base by chemical etching, to the working layer composition. The diagnostics result is shown in Fig. 2, which demonstrates, at the same scale, the experimental diagrams of the azimuthal angular dependence of the SHG signal from the outer graded band-gap base in the MCT180130 (a) heterostructure, after its removal by chemical etching (b) and from the GaAs substrate of this heterostructure (c). Note that from that point onward, where necessary, the quantitative characteristics of the studied objects are indicated in the captions to respective figures.

The Figure shows that the magnitude of the SHG signal reflected from the surface of the outer graded-gap wide-band MCT layer with a high cadmium content is 1.5 times smaller than the corresponding SHG signal reflected from the working layer surface. Those SHG signals from the MCT structures are more than by an order of magnitude greater than the reflected SHG signal from the back side of the sample, i.e., from the GaAs substrate.

Based on those and other data obtained, and with due account for the experimentally recorded opacity of the MCT layer for the exciting radiation at $\lambda = 1.064\,\mu$m (it is worth reminding that the amplitude penetration depth does not exceed $0.2\,\mu$m, and the SHG amplitude absorption length makes $\leq 0.03\,\mu$m), it can be stated that the SHG signals from the MCT heterostructure layers and from the GaAs substrate are purely reflected, with no contribution of the re-reflected laser radiation from the back surface of the sample substrate. Thus, the observed difference in the SHG signals amplitude in Fig. 2 and considering the characteristic second harmonic absorption amplitude length in the gallium arsenide substrates $\approx 0.15\,\mu$m indicates that the components of the nonlinear susceptibility tensor $\chi_{xyz}(\omega)$ at the wavelength of $\sim 1\,\mu$m of the MCT crystal heterostructure are by more than an order of magnitude greater than those of the CdTe and GaAs crystal heterostructures presented in [1].

3.2. Detecting the presence effect of disoriented microareas in MCT layers

When diagnosing the near-surface layers of certain tested MCT heterostructures and during layer-by-layer chemical etching, an increase of the noise was observed in the experimental diagrams of the azimuthal dependence of the SHG signal exceeding the noise level of the entire instrumental path. That increase was especially visible in the region of SHG signal minima (a kind of zero−method). It is not our task in this paper to determine the priority of the first works applying the zero−method while studying the SHG signals, note that various modifications of such diagnostic technique for any type of physical heterogeneities based on „forbidden" SHG signals have been widely used since the 80s of the previous century to date (see, for example, [27,28]). That noise increase can be attributed to the presence in the measurement region (incident radiation diameter is $\sim 200\,\mu$m) of disoriented microareas that cause the generation of a non-zero SHG signal in case of azimuthal orientation of the polarization of the main radiation and the second harmonic, especially in the minimum region where an ideal mono-crystal does not generate such SHG polarization. For most measurable MCT heterostructures, the noises of the azimuthal dependence of the SHG signal were limited by the noises of the measurement path. Thus, we classify the observed effects as the presence/absence of disordered microareas. Figure 3 shows, on an equal scale, the primary experimental diagrams of the azimuthal

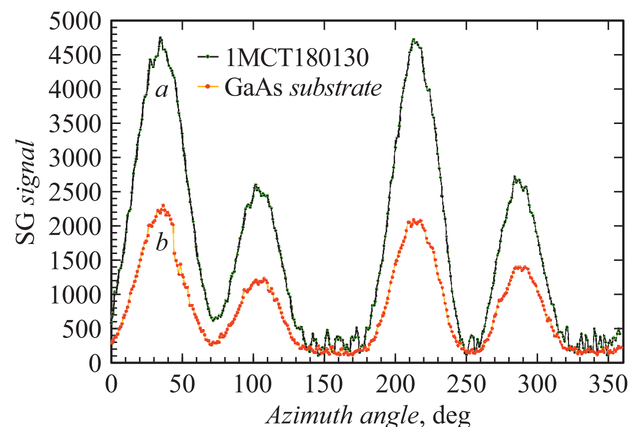

Figure 3. Experimental diagrams of the azimuthal dependence of the SHG signal from the MCT180130 heterostructure: a — after chemical etching to a depth of $\sim 5\,\mu$m; b — from the GaAs substrate. The average power of radiation at $\lambda = 1.064\,\mu$m is equal to 0.06 W. The polarizations of SHG and laser radiation are parallel.

dependence the SHG signal from the surface of the 180130 MCT sample layer after chemical etching to a depth of $\sim 5\,\mu$m (a) and from the GaAs substrate of that sample (b).

3.3. Stress diagnostics in MCT layers and the substrate material

Stresses in heterostructures and substrates were monitored for the availability of pronounced asymmetry in the experimental diagrams of the minima of the angular dependence and change (rise) of their levels [5,11]. The measurements taken on a highly sensitive NOLD bench revealed the same pattern of changes in the angular dependence of the SHG signals.

Let us evaluate the effect of deformations in semiconductor samples on the polarization characteristics of the laser radiation after passing through the sample based on the proposed weak-stress model [14].

The weak stress effect is related to the availability of deformations introduced into the sample during its growth or processing. The mechanical stresses appearing in the crystal are small and cannot affect the symmetry class or the orientation of the crystallographic axes in the sample, but they do affect the polarization properties of the laser radiation propagating in the crystal. The incident linearly polarized wave inside the crystal becomes elliptically polarized. The medium is a uniaxial crystal with slightly different refractive indices along the optical axis and in the directions perpendicular to the axis. The wave ellipticity after its interaction with the crystal is determined by the difference in refraction indices and depends on the magnitude of stresses at a given point; the ellipse spatial orientation is determined by the distribution of mechanical stresses in the sample.

Let us assume that the specimen transparent to the radiation incident normally along the Z axis on the plate has a weak transverse deformation with the n_e refraction index along it, and such index of n_o in the transverse direction, directed at β angle to the axis of the laboratory coordinate system Y. The Jones vector of incident radiation with an azimuthal angle of polarization α is

$$\begin{pmatrix} V_x \\ V_y \end{pmatrix} = E_o \begin{pmatrix} \cos\alpha \\ \sin\alpha \end{pmatrix}. \tag{1}$$

Let us compute the Jones matrix for the sample. Both ordinary and extraordinary waves propagate in the sample. $R(\beta)$ is the transition matrix from the laboratory coordinates to the system associated with the polarization vectors of those waves.

$$R(\beta) = \begin{pmatrix} \cos\beta & \sin\beta \\ -\sin\beta & \cos\beta \end{pmatrix},$$

hence, in the coordinates associated with the polarization vectors of ordinary and extraordinary waves,

$$\begin{pmatrix} V_o \\ V_e \end{pmatrix} = R(\beta) \begin{pmatrix} V_x \\ V_y \end{pmatrix}.$$

As the ordinary and extraordinary waves are orthogonal, the Jones matrix in the coordinate system associated with those vectors should be a diagonal one,

$$D = \begin{pmatrix} d_o & 0 \\ 0 & d_e \end{pmatrix},$$

where the d_i factors carry information about the changes in the amplitude and phase of the waves as they pass through the sample. As the refraction index of semiconductors has a large value ($n_o \sim 3$), the Jones matrix was calculated with due account for the multiple-beam interference of ordinary and extraordinary waves due to the re-reflection from the front and back surfaces of the sample. With due account for multiple reflections,

$$d_i \sim \frac{1}{1 - \alpha_i^2 \exp(-2jk_i h)}.$$

Here, $i = o, e$ are the indices indicating the wave type, k_i are the wave vectors, h is the sample thickness, α is the amplitude reflectivity, j is an imaginary unit,

$$\alpha_i = \frac{n_i - 1}{n_i + 1}.$$

The Jones matrix in the laboratory coordinates will look like that:

$$D = \begin{pmatrix} d_o \cos^2\beta + d_e \sin^2\beta & \frac{1}{2}(d_o - d_e)\sin 2\beta \\ \frac{1}{2}(d_0 - d_e)\sin 2\beta & d_e \cos^2\beta + d_e \sin^2\beta \end{pmatrix}. \tag{2}$$

The Jones vector of the probing radiation after passing the specimen or reflecting from it looks as follows:

$$\begin{pmatrix} V_x \\ V_y \end{pmatrix} = \\ = E_o \begin{pmatrix} \cos\alpha(d_o\cos^2\beta + d_e\sin^2\beta) + \sin\alpha\,\frac{1}{2}(d_o - d_e)\sin 2\beta \\ \sin\alpha(d_o\cos^2\beta + d_e\sin^2\beta) + \cos\alpha\,\frac{1}{2}(d_o - d_e)\sin 2\beta \end{pmatrix}. \tag{3}$$

The appearance of the second addends in the polarization components of the Jones vector (3) can lead to structural changes of the SHG azimuthal dependences in the diagrams, namely, to level elevation of several minima and the appearance of their asymmetry.

Note that such effect of SHG signal modification due to the stresses has been intensively used recently, for calculating and mapping the stress fields in various kinds of structures (see, for example, [27]).

Numerous comparative experiments showed that the meaningful influence of the stress fields in GaAs substrates and MCT structures on the position and relative magnitude of the SHG signal maxima in the azimuthal diagrams, when compared against similar model dependences for an ideal mono-crystal, is much less pronounced due to the smallness of the induced birefringence effect itself.

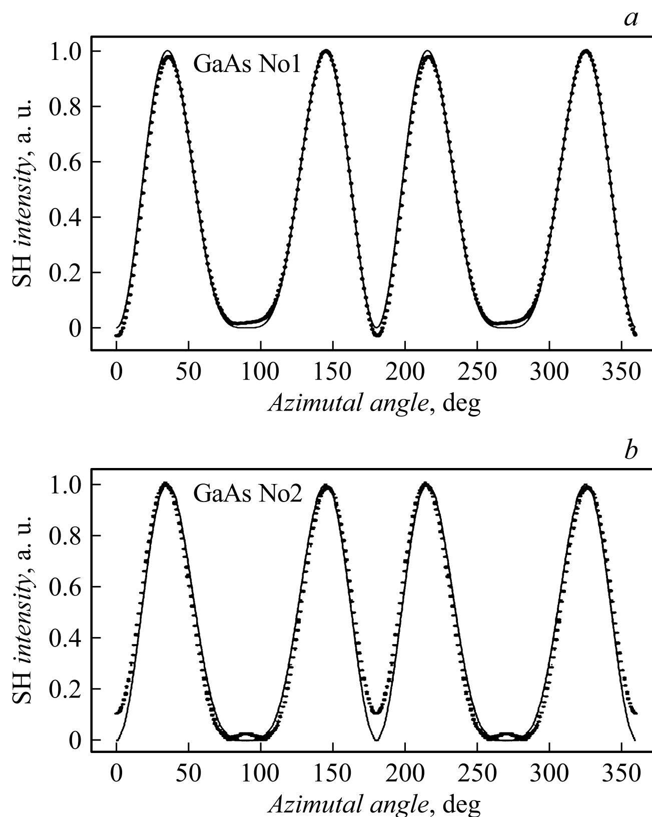

Figure 4. The comparison results of the experimental SHG signal intensity diagram (dotted line, high frequency array cleanup was performed) against the theory (solid line) for № 1 (a) and № 2 (b) GaAs substrates. The deviation from the orientation (013) in φ angle is less than 1°. Stresses in the № 1 substrate are weak (no asymmetry and rises in the experimental graph), and strong in № 2 substrate. The average power of radiation at $\lambda = 1.064\,\mu$m is 0.06 W. The polarizations of SHG and laser radiation are parallel.

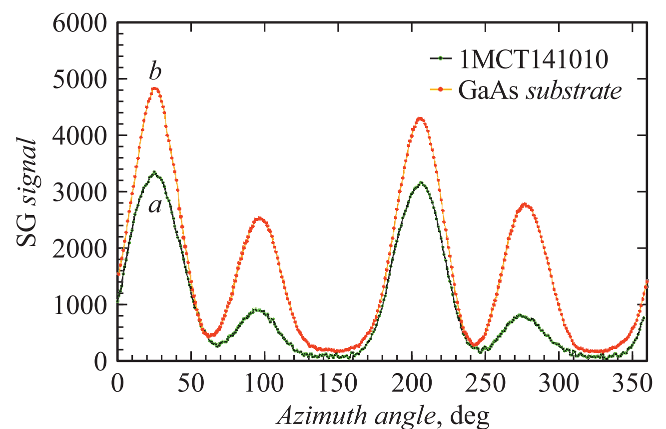

Figure 5. Experimental diagrams of the azimuthal dependence of the SHG signal on the 141010 (a) MCT sample and on the GaAs substrate of this heterostructure (b). The average power of radiation at $\lambda = 1.064\,\mu$m for it a is 0.04 W, for b is 0.13 W. The polarizations of the SHG and the laser radiation are parallel. Noticeable similar stresses are visible in the structure and substrate (pronounced asymmetry and different levels of minima of the angular dependence in the experimental diagram).

As vivid examples, we use the illustrations of the experimental diagrams of SHG azimuthal dependence as compared against the model dependences for an ideal stressless mono-crystal.

The experimental and model angular dependences of the SHG signal on the samples were compared programmably, using an array of model angular dependences with a variation for the φ angle in 1° — this is the error of the experimental results in this paper.

Figure 4 shows the experimental and model angular dependences of the SHG signal magnitude from two GaAs substrates: a — № 1 (without significant stresses) and b — № 2 (obvious presence of stresses). Here, the experimental diagram is a dotted line (a high-frequency cleanup of the experimental array was performed), the theoretical angular dependence is a solid line.

In the same way, it was unambiguously established on a large experimental material that characteristic change in the behavior of the SHG signal azimuthal dependences due to stresses in the substrate also manifests itself in the same way in the heterostructure layers put on that substrate. Figure 5 clearly demonstrates this fact. Here, for the 141010 MCT specimen, the azimuthal dependences are shown of the SHG signal on the front side of the (a) MCT heterostructure and on the back side (GaAs substrate) of this sample. When comparing the diagrams, it is evident that the substrate stresses are manifested in the SHG signal, to the uppermost layers of the MCT heterostructure, which, among other things, increased the deviation in orientation from (013) as compared to the substrate by $\sim 4^\circ$ for angle φ. For the sake clarity of visual comparison of the two experimental diagrams' minima, the average power of the exciting radiation during the SHG registration from the substrate was tripled (consequently, the SHG signal increased by approximately an order of magnitude).

In this paper we only draw the attention to the potential of the SHG method to unambiguously fix the availability/non-availability of significant stresses in the substrate material and in the layers of heterostructures on it, and we also assume that the azimuthal dependences can be calculated of the SHG signal in a stressed crystal by perturbation method, using the weak induced birefringence method.

3.4. Effects of high power probing radiation (local short-term radiant heating) on the characteristics of the crystalline state of MCT structures and layers

As the MCT heterostructures are opaque to the exciting radiation and to its second harmonic, we used the *in situ* effects of the laser radiation power to determine the threshold power value when the changes begin in the crystal characteristics of the MCT layer surface of the grown

heterostructure. The crystalline state was measured of the near-surface region of the outer graded-band gap layer of the MCT heterostructure (composition of 0.45 CdTe molar fractions). It was found experimentally that the effect of laser radiation power begins affecting the crystalline characteristics already at the power of ~ 0.2 W and above (the area of $200\,\mu$m in diameter). Fig. 5 shows the initial azimuthal dependences of the SHG signal characterizing the crystalline state of the MCT surface and the back side of 141010 MCT heterostructure substrate, at the probing radiation power of 0.04 and 0.13 W, respectively.

At higher powers, changes in the crystalline state of the near-surface MCT layer were observed. Fig. 6 shows the data on exposure to 0.3 W exciting radiation while recording the azimuthal dependence of the SHG signal for 60 s. To prove that the fine structure of the azimuthal dependences in Fig. 6 is not related to the ADC noises (± 16 units of ADC code), the amplitude of the recorded SHG signal is given in ADC codes. It follows from the above results that the exposure for 194 s decreases the amplitude of the SH signal in the maxima and increases the noises in the minima (Fig. 6, *c*). This means that over that time, a local short-term heating takes place by exciting radiation until a physical change takes place of the crystalline state which never fully recovers to its original state. Indeed, during local near-surface zone heating from the initial state (Fig. 6, *a*), it was gradually losing the symmetry properties of its class while maintaining the overall noncentrosymmetry of the heterostructure (Fig. 6, *b*, *c*), there appeared disordered microareas of the MCT heterostructure (see Sect. 3.2), that were providing a diffusion component to the SHG signal. So, the local laser annealing is observed, in which the crystalline state of the material can be changing its state until the amorphous phase appears, as shown in [1]. Questions relating to the modification of the heterostructure layers properties under exposure and about the final crystalline characteristics of the irradiated zone upon laser exposure are a subject of further research.

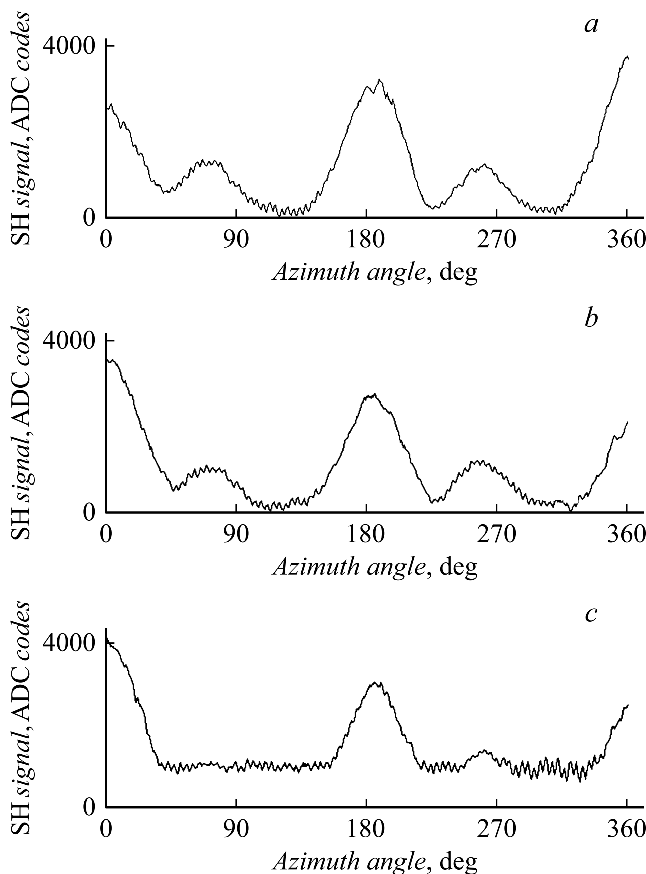

Figure 6. Azimuthal dependences of the SHG signal from the same point on the 141010 MCT sample face (normal incidence, $s-s$-geometry, consistent continuous history of $a-c$ diagrams, recording time of each diagram is 60 s, the interval between the diagrams is ~ 7 s). The power of the continuous exciting radiation within that time interval was ~ 0.3 W.

Conclusion

The results are presented of creating and applying highly sensitive express nonlinear optical diagnostics based on the second harmonic generation method and the measurements of azimuthal angular dependences of the polarization components of the signal reflected from the SHG sample on the probing laser radiation. The sensitivity of nonlinear optical diagnostics was enhanced in order to obtain more informative characterization of sphalerite-type crystals. New experimental results were obtained related to the crystalline quality of the MBE-grown MCT heteroepitaxial structure and the sublayer material.

Research of cadmium-mercury-telluride solid solution heterostructures MBE-grown on GaAs substrates using a high-sensitivity NOLD bench confirmed the influence of stresses on the pronounced asymmetry of the angle dependence minima of the experimental SHG signal diagrams in GaAs substrates and MCT layers. Similar manifestation was registered in the diagrams of SHG signal of stresses in the substrate material and in the layers of the grown MCT heterostructure.

The registered SHG signal as reflected from HgCdTe layers and GaAs substrate confirmed that the $\chi_{xyz}(\omega)$ nonlinear susceptibility value of MCT depends on the composition of MCT layers and exceeds, at least by an order of magnitude, a similar value for CdTe and GaAs at the $\sim 1\,\mu$m laser emission wavelength. The nonlinear susceptibility value for MCT layers of 0.22 molar percentage of CdTe exceeds the same value for MCT layers of 0.45 molar percentage of CdTe.

The effect of noise enhancement was revealed in the azimuthal dependence minima in the MCT layers of certain heterostructures, significantly exceeding the noise of the measurement path. We attribute such behavior to the availability of disordered microareas in the MCT heterostructure layers, that being observed for the first time.

The threshold value was identified for the exciting radiation power of less than 0.2 W, at which no changes are observed in the crystalline state in the MCT layers,

this confirming the correctness of crystalline structure state measurements after growth.

At higher powers of $\sim 0.2-0.3$ W a local short-term radiant heating is observed, leading to changes in the crystalline structure of the layers in the MCT heterostructure. The phenomenon was observed *in situ* due to simultaneous measurements of the azimuthal dependences of the SHG signal. In this way the crystalline structure state can be changed under control, and local modification of material properties can be implemented.

It is shown that the crystalline state characterization method of the MCT structures and layers by the second harmonic allows express support to creation of MCT semiconductor heterostructures in order to achieve their required quality in subsequent applications.

Acknowledgments

The work was partially supported by the Russian Foundation for Fundamental Research (project № 18-29-20053), Volkswagen Stiftung Program (№ 97738), and as part of the state assignment of the Russian Federal Ministry of Education and Science in terms of project AAAA-A20-120102190007-5.

Conflict of interest

The authors declare that they have no conflict of interest.

References

[1] S.A. Akhmanov, V.I. Yemelyanov, N.I. Koroteev, V.V. Seminogov. Sov. Phys. Usp, **28**, 1084 (1985). DOI: 10.1070/PU1985v028n12ABEH003986

[2] T.F. Heinz. *Second-Order Nonlinear Optical Effects at Surfaces and Interfaces. In: Nonlinear Surface Electromagnetic Phenomena.* Eds H. Ponath, G. Stegeman. (North Holland Pub., Amsterdam, 1991)

[3] T. Kimura, Ch. Yamada, J. Crystal Growth, **150**, 92 (1995).

[4] K.A. Brekhov, K.A. Grishunin, D.V. Afanasyev, S.V. Semin, N.E. Sherstyuk, Y.D. Mishina, A.V. Kimel. Phys. Solid State, **60**, 31 (2018). DOI: doi.org/10.1134/S1063783418010080

[5] V.V. Balanyuk, V.F. Krasnov, S.L. Musher, V.I. Prots, V.E. Ryabchenko, S.A. Stoyanov, S.G. Struts, M.F. Stupak, V.S. Syskin. Quantum Electron, **25**, 2 183 (1995). DOI: 10.1070/QE1995v025n02ABEH000320

[6] G.M. Borisov, V.G. Goldort, A.A. Kovalev, S.A. Kochubey, D.V. Ledovskikh, V.V. Preobrazhenskiy, M.A. Putyato, N.N. Rubtsova, B.R. Semyagin. Vestn. Novosib.gos.un-ta. (in Russian) Seriya: Fizika, **4** (5), 2014. (in Russian).

[7] G.M. Borisov, V.G. Goldort, K.S. Zhuravlev, A.A. Kovalev, S.A. Kochubey, D.V. Ledovskikh, T.V. Malin, N.N. Rubtsova. Sibirskiy fizicheskiy zhurnal, **13** (2), 64 (2018).(in Russian) DOI: 10.25205/2541-9447-2018-13-2-64-69

[8] S.B. Bodrov, A.I. Korytin, Yu.A. Sergeev, A.N. Stepanov. Quant. Electron., **50** (5), 496 (2020). DOI: http://dx.doi.org/10.1070/QEL17185

[9] I.D. Burlakov, A.V. Demin, G.G. Levin, N.A. Piskunov, S.V. Zabotnov, A.S. Kashuba. Meas Tech, **53**, 615–619 (2010). DOI: 10.1007/s11018-010-9550-6

[10] Y.V. Permikina, A.S. Kashuba. Uspekhi prikladnoi fiziki, **4** (5), 493 (2016).(in Russian).

[11] M.F. Stupak, N.N. Mikhailov, S.A. Dvoretskii, M.V. Yakushev, D.G. Ikusov, S.N. Makarov, A.G. Elesin, A.G. Verkhoglyad. Physics of the Solid State, **62** (2), 252 (2020). DOI: 10.1134/S1063783420020201

[12] V.V. Pavlov, A.M. Kalashnikova, R.V. Pisarev, I. Sanger, D.R. Yakovlev, M. Bayer. J. Opt. Soc. Am. B, **22**, 168 (2005).

[13] M. Fiebig, V.V. Pavlov, R.V. Pisarev. J. Opt. Soc. Am. B, **22**, 96 (2005).

[14] S.L. Musher, M.F. Stupak, V.S. Syskin. Quantum Electron, **26** 743 DOI: 10.1070/QE1996v026n08ABEH000768

[15] A. Rogalski. Rep. Prog. Phys., **68**, 2267 (2005).

[16] Yu.G. Sidorov, S.A. Dvorestkiy, V.S. Varavin, N.N. Mikhailov, M.V. Yakushev, I.V. Sabinina. Semiconductors, **35**, 9, 1045 (2001). DOI: 10.1134/1.1403569

[17] Yu.G. Sidorov, M.V. Yakushev, A.V. Kolesnikov. Optoelectron. Instrument. Proc. **50**, 234 (2014). DOI: 10.3103/S8756699014030030

[18] Yu.G. Sidorov, M.V. Yakushev, V.S. Varavin, A.V. Kolesnikov, E.M. Trukhanov, I.V. Sabinina, I.D. Loshkarev. Phys. Solid State, **57**, 2151 (2015). DOI: 10.1134/S1063783415110311

[19] D. Chandra, H.D. Shih, F. Aqariden, R. Dat, S. Gutzler, M.J. Bevan, T. Orent. J. Electron. Mater., **27** (6), 640 (1998).

[20] L. He, Y. Wu, L. Chen, S.L. Wang, M.F. Yu, Y.M. Qiao, J.R. Yang, Y.J. Li, R.L. Ding, Q.Y. Zhang. J. Cryst. Growth, **227**–**228**, 677 (2001).

[21] J.D. Benson, L.O. Bubulac, P.J. Smith, R.N. Jacobs, J.K. Marcunas, M. Jaime-Vasques, L.A. Almeida, A.J. Stoltz, P.S. Wijewarnasuriya, G. Brill, Y. Chen, U. Lee, M.F. Vilela, J. Peterson, S.M. Johnson, D.D. Lofgreen, D. Rhiger, E.A. Patten, P.M. Goetz. J. Electron. Mater., **39** (7), 1080 (2010).

[22] V.I. Gavrilenko, A.M. Grekhov, D.V. Korbutyak, V.G. Litovchenko. *Opticheskiye svoistva poluprovodnikov. Spravochnik* (Naukova dumka, Kiev, 1987) (in Russian)

[23] *Handbook of Optical Constants of Solids*. Ed. by E.D. Palik. (Elsevier Science, USA, 1998)

[24] *Optical Constants of Crystalline and Amorphous Semiconductors*. Sadao Adachi. (Springer Science+ Business Media, NY., 1999)

[25] E.D. Mishina, T.V. Misuryaev, N.E. Sherstyuk, V.V. Lemanov, A.L. Morozov, A.S. Sigov, Th. Rasing. Phys. Rev. Lett., **85**, 3664 (2000).

[26] E.D. Mishina, A.I. Morozov, A.S. Sigov, N.E. Sherstyuk, O.A. Aktsipetrov, V.V. Lemanov, Th. Rasing. J. Exp. Theor. Phys, **94**, 552 (2002). DOI: 10.1134/1.1469155

[27] L. Mennel, M.M. Furchi, S. Wachter, M. Paur, D.K. Polyushkin, Th. Mueller. Nat. Commun., **9**, 516 (2018). DOI: 10.1038/s41467-018-02830-y

[28] B.R. Carvalho, Y. Wang, K. Fujisawa, T. Zhang, E. Kahn, I. Bilgin, P.M. Ajayan, A.M. de Paula, M.A. Pimenta, S. Kar, V.H. Crespi, M. Terrones, L.M. Malard. Nano Lett., **20** (1), 284 (2020). DOI: 10.1021/acs.nanolett.9b03795